Astron. Astrophys. 339, 123–133 (1998)

ASTRONOMY AND ASTROPHYSICS

The evolution of helium white dwarfs

I. The companion of the millisecond pulsar PSR J1012+5307⋆

T. Driebe[1,2], **D. Schönberner**[2], **T. Blöcker**[1,3], **and F. Herwig**[2]

[1] Max-Planck-Institut für Radioastronomie, Auf dem Hügel 69, D-53321 Bonn, Germany (driebe@speckle.mpifr-bonn.mpg.de; bloecker@speckle.mpifr-bonn.mpg.de)
[2] Astrophysikalisches Institut Potsdam, An der Sternwarte 16, D-14482 Potsdam, Germany (deschoenberner@aip.de; fherwig@aip.de)
[3] Institut für Theoretische Physik und Astrophysik, Universität Kiel, D-24098 Kiel, Germany

Received 6 February 1998 / Accepted 8 July 1998

Abstract. We present a grid of evolutionary tracks for low-mass white dwarfs with helium cores in the mass range from 0.179 to $0.414\ \mathrm{M}_\odot$. The lower mass limit is well-suited for comparison with white dwarf companions of millisecond pulsars. The tracks are based on a $1\ \mathrm{M}_\odot$ model sequence extending from the pre-main sequence stage up to the tip of the red-giant branch. Applying large mass loss rates at appropriate positions forced the models to move off the giant branch. The further evolution was then followed across the Hertzsprung-Russell diagram and down the cooling branch. At maximum effective temperature the envelope masses above the helium cores increase from 0.6 to $5.4 \cdot 10^{-3}\ \mathrm{M}_\odot$ for decreasing mass. We carefully checked for the occurrence of thermal instabilities of the hydrogen shell by adjusting the computational time steps accordingly. Hydrogen flashes have been found to take place only in the mass interval $0.21 \lesssim M/\mathrm{M}_\odot \lesssim 0.3$.

The models show that hydrogen shell burning contributes significantly to the luminosity budget of white dwarfs with helium cores. For very low masses the hydrogen shell luminosity remains to be dominant even down to effective temperatures well below $10\,000\,\mathrm{K}$. Accordingly, the corresponding cooling ages are significantly larger than those gained from model calculations which neglect nuclear burning or the white dwarf progenitor evolution.

Using the atmospheric parameters of the white dwarf in the PSR J1012+5307 system we determined a mass of $M = 0.19 \pm 0.02\ \mathrm{M}_\odot$ and a cooling age of $6 \pm 1\mathrm{Gyr}$, in good agreement with the spin-down age, 7 Gyr, of the pulsar.

Key words: stars: evolution – stars: interiors – white dwarfs – binaries: general – pulsars: individual: PSR J1012+5307

1. Introduction

The theory of stellar evolution shows that white dwarfs (WD) with a carbon-oxygen core (CO-WDs) can be well understood in terms of the evolution of single stars with initial masses between 1 and about $6 \ldots 8\,\mathrm{M}_\odot$. After central hydrogen burning, stars in this mass range develop first a helium core surrounded by a hydrogen-burning shell (red-giant branch or RGB) and later, after completion of central helium burning, a compact carbon-oxygen core surrounded by two shells burning hydrogen and helium, respectively (asymptotic giant branch or AGB). At high luminosities strong stellar winds erode the stellar envelope effectively. When the envelope mass drops below a few $10^{-2}\ \mathrm{M}_\odot$ the model leaves the AGB, becomes a central star of a planetary nebula and finally cools down as a white dwarf. The final masses range typically between about 0.5 and $1\ \mathrm{M}_\odot$ (see e.g. Iben & Renzini 1983; Schönberner 1979, 1983; Vassiliadis & Wood 1993, 1994; Blöcker 1995a, 1995b).

White dwarfs with smaller masses cannot be produced by single-star evolution since their progenitors would have initial masses below $0.5\,\mathrm{M}_\odot$ and thus do not finish their main sequence evolution within a Hubble time. Instead one has to invoke mass transfer in a close binary system whereby the donor's evolution towards central helium ignition is choked off – the so-called case B mass exchange (Kippenhahn & Weigert 1967). The remnant is a low-mass object ($M < 0.5\ \mathrm{M}_\odot$), consisting of a helium core with a hydrogen-rich envelope still burning hydrogen at its bottom, which contracts slowly towards a white dwarf configuration, quite similar to the more massive and more luminous remnants from the AGB.

Two known common types of binary systems can contain such helium white dwarfs (He-WDs). Firstly the so-called double-degenerate systems, where both components are white dwarfs (see e.g. Saffer et al. 1998). Examples for such systems with one or even two He-WDs are WD 0957-666 (Bragaglia et al. 1990; Moran et al. 1997), WD 0135-052 (= L870-2 = EG11, Saffer et al. 1988), PG 1101+364 (= Ton 1323, Marsh 1995) and the five systems studied by Marsh et al. (1995). The second type are the so-called millisecond pulsar systems (hereafter MSP), where the He-WD is the companion of a pulsar with a high rotational speed in a nearly circular orbit.

So far about three dozens of these systems are known. Most of them have a low-mass white dwarf companion (see for ex-

Send offprint requests to: T. Driebe

⋆ Tables 5-11 are only available in electronic form at the CDS via ftp 130.79.128.5

ample Bailes & Lorimer 1995, Camilo et al. 1996, Ray et al. 1996, Lyne 1996). Reviews of MSP properties are given, e.g., by Verbunt (1993), Shore et al. (1994), Phinney & Kulkarni (1994), Rappaport et al. (1995), Nicastro et al. (1995), Camilo (1996) or Lyne (1995). The evolution of the progenitor system can be explained by highly non-conservative mass exchange events (common envelope evolution). A detailed description of the binary scenario which leads to the formation of a MSP system has recently been given, e.g., by Tauris & Bailes (1996), Tauris (1996) or Ergma & Sarna (1996). In progenitor systems to MSPs the more massive component ($M_1 \approx 10\ \mathrm{M}_\odot$) fills its Roche volume, looses a substantial amount of mass but follows the evolution towards a supernova explosion with the formation of a neutron star which might be detected as a radio pulsar. The less massive secondary component ($M_2 \approx 1\ \mathrm{M}_\odot$) continues its evolution, evolves off the main sequence to become a red giant and will eventually also exceed its Roche lobe to spill its mass onto the neutron star. This accretion of matter spins up the neutron star to rotational periods of the order of milliseconds. In this phase the system can be identified as a low mass X-ray binary system (LMXB) like Cyg X-2 or 2S 0921-63 (Webbink et al. 1983; Verbunt 1993; for a population synthesis of LMXBs see Iben et al. 1995). Continuing mass exchange of the secondary causes its envelope mass to fall below a critical value. The system becomes detached again, and the secondary evolves to a white dwarf with a helium core while the pulsar's rotation slows down again by energy loss at the expense of rotational energy and the pulsar properties are activated again.

Using smaller initial mass ratios the scenarios for the emergence of MSs also describe, in principle, the formation of double degenerate systems, i.e. systems containing two white dwarfs (CO+CO, He+CO, He+He). For a discussion of these systems see for example Webbink (1984), Iben & Tutukov (1984a, 1986), Cameron & Iben (1986) and, more recently, Sarna et al. (1996).

MSP systems open the unique possibility to check the spin-down theory of pulsars by independent age determinations of the white dwarf components once the atmospheric parameters of the latter are known. PSR J1012+5307 is so far the only system where the white dwarf has been studied with sufficient precision as to allow for comparing spin-down and cooling ages (see e.g. Lorimer et al. 1995) and to determine the components' masses.

PSR J1012+5307 was identified by Nicastro et al. (1995). They found a rotational period $P_{\mathrm{rot}} = 5.26\ \mathrm{ms}$ and a compact companion with a minimum mass of 0.11 $\mathrm{M}_\odot$ in an orbit with period $P_{\mathrm{orb}} = 14.5\,\mathrm{h}$. The surface parameters of the companion have been determined by van Kerkwijk et al. (1996) and Callanan et al. (1998). Due to different atmospheric models the derived parameters differ somewhat: van Kerkwijk et al. (1996) found $\log g = 6.75 \pm 0.07$ and $T_{\mathrm{eff}} = 8550 \pm 25\,\mathrm{K}$ while Callanan et al. (1998) give $\log g = 6.34 \pm 0.20$ and $T_{\mathrm{eff}} = 8670 \pm 300\ \mathrm{K}$. According to these atmospheric parameters the companion is a low-mass helium white dwarf as suggested by the theoretical scenarios sketched above. Van Kerkwijk et al. (1996) estimated a mass of $0.16 \pm 0.02\ \mathrm{M}_\odot$ by extrapolating from more massive carbon-oxygen models. The same result was found by Callanan et al. (1998) from their analysis and white dwarf modelling.

Lorimer et al. (1995) determined the spin-down age $\tau = 7.0$ Gyr assuming $P_0 \ll P_{\mathrm{rot}}$, where P_0 is the initial pulsar period after the end of the spin-up phase. The age of the MSP can be estimated as well by the cooling age of the WD companion. However, the estimates based on existing white dwarf calculations are controversial: while Lorimer et al. (1995) derived a cooling age for the white dwarf of about 0.3 Gyr, which is a factor 20 lower than the pulsar's spin-down age, Alberts et al. (1996) give a value of 7 Gyr, in full agreement with the spin-down age of the pulsar.

To solve the problem of age determination of MSPs two different strategies are possible: The first concerns the critical examination of the spin-up and spin-down theories for pulsars. On one hand, an uncertainty in the spin-down age determination arises from the assumption $P_0 \ll P$. Violations of this assumption result in lower spin-down ages (see for example Camilo et al. 1994). On the other hand, Burderi et al. (1996) showed that by assuming an accretion-induced field decay instead of spontaneous field decay substantially lower spin-down ages can be obtained. Following their conclusions MSP systems would thus have characteristic ages of a few 10^8 years only. In the particular case of PSR J1012+5307 Burderi et al. (1996) found a spin-down age of about $3.7 \cdot 10^8$ yr.

The other strategy for deriving corresponding ages involves the reexamination of the evolutionary models of low-mass white dwarfs. Studies of such objects are rare, in particular for $M < 0.2\ \mathrm{M}_\odot$ as is appropriate for PSR J1012+5307. Several authors, i.e. Kippenhahn et al. (1967), Kippenhahn et al. (1968), Refsdal & Weigert (1969), Gianonne et al. (1970), Iben & Tutukov (1986) and Castellani et al. (1994) computed models of He-WDs with $M > 0.2\ \mathrm{M}_\odot$ by simulating mass exchange in close binaries. Typical is that all of these studies have encountered thermal instabilities (or hydrogen flashes) in models with $M > 0.25\,\mathrm{M}_\odot$ due to unstable hydrogen burning on the cooling branch.

Chin & Stothers (1971) and Webbink (1975) constructed He-WD models by following the evolution of single stars of the appropriate low masses. Webbink (1975) calculated a grid of sequences in the mass range $0.1 < M/\,\mathrm{M}_\odot < 0.5$. However, due to large time steps used his tracks do not show any thermal instabilities. From Webbinks calculations one can infer that the white dwarf companion in the PSR J1012+5307 system should have an age of $\tau \approx 10$ Gyr. Chin & Stothers (1971) did not include hydrogen shell burning in their white dwarf models. According to their $M = 0.2\ \mathrm{M}_\odot$ track, the white dwarf in the PSR J1012+5307 system is only 0.3 Gyr old. Hereafter, models with the explicit assumption $L_{\mathrm{nuc}} = 0$ will be referred to as contraction models.

Alberts et al. (1996) calculated He-WD models between $0.17 < M/\,\mathrm{M}_\odot < 0.25$ by simulating binary evolution with low-mass components. They found no thermal instabilities of the hydrogen burning shell. Their models give for the PSR J1012+5307 companion's mass and age $M = 0.185\ \mathrm{M}_\odot$ and $\tau = 7$ Gyr, respectively.

Althaus & Benvenuto (1997) and Benvenuto & Althaus (1998) presented models in the mass range $0.15 < M/\,\mathrm{M}_\odot < 0.5$. Althaus & Benvenuto (1997) treated He-WDs without any hydrogen envelopes, and thus did not allow for nuclear burning. Benvenuto & Althaus (1998) and Hansen & Phinney (1998a) ($0.1 < M/\,\mathrm{M}_\odot < 0.5$) started their calculations considering hydrogen burning, but found it to be insignificant. All sets of tracks of these authors display very similar cooling properties, and one can estimate a cooling age of about $\tau \lesssim 0.5$ Gyr for the white dwarf in the PSR J1012+5307 system. Note, that, however, their initial models differ from those based on calculations of RGB progenitors with mass loss.

It is obvious from this comparison that the cooling properties of low-mass white dwarfs are extremely sensitive to the initial conditions. We suggest that initial models closest to real He-WD progenitors result from explicit modeling of their evolutionary history which determines the model's envelope mass and thermomechanical structure. Therefore we have calculated an extensive grid of model sequences with full consideration of nuclear burning. Our investigations revealed that the simultaneous consideration of these two aspects, i.e. nuclear burning and the evolutionary history, results in considerably longer evolutionary ages of the white dwarfs. Consequences for the mass determination are evident as well. A full presentation of this evolutionary grid, with an extensive discussion of thermal instabilities and the mass-radius relation is deferred to a forthcoming paper. Here we will discuss only those model properties that are important to interpret millisecond pulsar systems.

This paper is organized as follows: in Sect. 2 we describe the stellar evolution code and the method used to calculate evolutionary models presented in this paper. Results are given in Sect. 3 and applied to the particular system PSR J1012+5307. Sect. 4 summarizes our results.

2. The evolutionary calculations

The evolutionary code used is essentially the one described by Blöcker (1995a), with several modifications. Nuclear burning is accounted for via a nucleosynthesis network including 30 isotopes with all important reactions up to carbon burning similar as in El Eid (1994). The most recent radiative opacities by Iglesias et al. (1992) and Iglesias & Rogers (1996) [OPAL], supplemented by those of Alexander & Ferguson (1994) in the low-temperature region, are employed. Diffusion is not considered. The initial composition is $(Y, Z) = (0.28, 0.02)$, the mixing length parameter $\alpha = 1.7$ follows from calibrating a solar model. The Coulomb corrections to the equation of state are those given by Slattery et al. (1982). We note in passing that for the results presented here the quality of the Coulomb correction treatment is of no significance.

For comparison we have also computed evolutionary sequences based on different input physics:

- sequences using the older opacities of Cox & Stewart (1965a, 1965b, 1970) [CS]; and
- sequences using equilibrium nuclear reaction rates for hydrogen and helium burning.

In the following we will only refer to the sequences based on the OPAL opacities with full employment of the nuclear network if not mentioned differently.

2.1. Method of calculation

Because we primarily focused our study on the cooling behaviour of low-mass white dwarfs and the implications for the mass-radius relation we did not calculate the mass exchange phases during the RGB evolution in detail (see for this subject, e.g., Tauris 1996, Tauris & Bailes 1996). Rather, for our purpose it was sufficient to simulate the mass-exchange episode by subjecting a RGB model to a sufficiently large mass loss rate (Iben & Tutukov 1986, Castellani et al. 1994). We emphasize that, once mass loss has been turned off, the model's further evolution does not depend on the details of the previous mass loss episode. The evolutionary speed across the Hertzsprung-Russell diagram is rather controlled by the model's structural changes caused by the actual envelope-mass reduction due to hydrogen burning and mass loss.

In order to get realistic starting models, we calculated a $1\,\mathrm{M}_\odot$ sequence from the pre-main sequence phase up to the tip of the RGB. Along the RGB we applied mass-loss rates $\dot{M}_\mathrm{R}$ according to Reimers (1975) with $\eta = 0.5$ as in Maeder & Meynet (1989). At appropriate positions high mass loss rates, $\dot{M}_\mathrm{high}$, were invoked in order to get models of desired final mass, M. Since in the actual situations Roche-lobe overflow is assumed to occur on a nuclear time scale, the maximum applied mass loss rate was chosen in such a way as not to destroy the model's thermal equilibrium. Accordingly, $\dot{M}_\mathrm{high}$ varied from $\dot{M}_\mathrm{high} \approx 10^{-9}\,\mathrm{M}_\odot\,\mathrm{yr}^{-1}$ for $M \approx 0.15\,\mathrm{M}_\odot$ to about $\dot{M}_\mathrm{high} \approx 10^{-6}\,\mathrm{M}_\odot\,\mathrm{yr}^{-1}$ for $M \approx 0.4\,\mathrm{M}_\odot$. Below a critical envelope mass, $M_\mathrm{env}^\mathrm{crit}$, sufficient densities and temperatures to continue hydrogen burning can only be maintained if the envelope contracts. Then, the model starts to leave the RGB. At this point of evolution mass loss was virtually switched off by decreasing $\dot{M}$ over a short transition period until $\dot{M} = \dot{M}_\mathrm{R}$ was reached. In general we chose $T_\mathrm{eff} = 5000$ K to be the point where $\dot{M}$ should have reached the Reimers rate with $\eta = 0.5$. For models with $M \lesssim 0.2\,\mathrm{M}_\odot$ we had to increase this temperature to $T_\mathrm{eff} = 10000$ K because models on the lower part of the RGB have temperatures still too close to $T_\mathrm{eff} = 5000$ K.

The critical envelope mass, $M_\mathrm{env}^\mathrm{crit}$, which marks the transition between expansion and contraction of the star's envelope, depends on the mass of the the hydrogen-exhausted core, M_c, in a way similar to what is found for post-AGB remnants: the larger the core, the smaller the residual envelope mass. When this value is reached, Roche-lobe contact will be shut off, and the remnant will continue its evolution with $L \approx L_\mathrm{Hyd} \approx \mathrm{const}$ and $\dot{R} < 0$ towards larger T_eff. The models' evolutionary speed is determined by the evolution of the envelope mass which is reduced both by hydrogen burning, i.e. the core growth rate $\dot{M}_\mathrm{c}$, and the mass loss rate, i.e. $\dot{M}_\mathrm{R}$ in the presented models. Since $\dot{M}_\mathrm{c}/\dot{M}_\mathrm{R} \sim 1/R$ mass loss becomes rapidly unimportant at least for $T_\mathrm{eff} > 10000$ K. The envelope mass at the turn-around

Table 1. Total remnant mass, M, mass of the hydrogen-exhausted core, $M_{\rm c}$, total mass of the outer hydrogen layers ("thickness"), $M_{\rm H}$, envelope mass, $M_{\rm env}$, and helium surface abundance by mass fraction, Y, at $T_{\rm eff} = 5000$ K for $M > 0.2{\rm M}_\odot$ and at 10000 K for $M \leq 0.2{\rm M}_\odot$ after the end of RGB evolution

$M/{\rm M}_\odot$	$M_{\rm c}/{\rm M}_\odot$	$\frac{M_{\rm H}}{10^{-3}{\rm M}_\odot}$	$\frac{M_{\rm env}}{10^{-3}{\rm M}_\odot}$	Y
0.179	0.1552	25.550	48.289	0.464
0.195	0.1782	16.766	30.768	0.462
0.234	0.2220	8.118	13.098	0.354
0.259	0.2524	4.771	7.232	0.312
0.300	0.2960	3.189	4.746	0.301
0.331	0.3281	2.509	3.744	0.301
0.414	0.4116	1.446	2.175	0.301

point at maximum effective temperature is independent of the post-RGB mass loss.

Our procedure is adequate for obtaining reliable starting models for He-WD tracks. Due to their evolutionary history the internal structure of these initial models is consistent with the one expected from binary evolution (see references in Sect. 1). This concerns the envelope masses as well. As will be shown in the following sections the latter has consequences for the mass-radius relation. Furthermore, the evolutionary envelope masses give rise to ongoing hydrogen shell burning during the white dwarf evolution. This greatly prolongs the cooling times of the He-WDs.

3. Results

We calculated seven evolutionary sequences starting at different locations along the RGB of the $1\ {\rm M}_\odot$ sequence. They are listed in Table 1, where we give the total amount of hydrogen contained in the envelope, the 'thickness' $M_{\rm H}$, the total envelope mass, $M_{\rm env}$, and the helium surface abundance by mass fraction, Y. Note, that $M_{\rm H} \approx 0.7\ M_{\rm env}$ except for the least massive remnants. For $M \lesssim 0.3{\rm M}_\odot$ mass loss has uncovered layers where hydrogen burning took place during the main sequence phase. Consequently, the helium surface abundance of those models amounts up to $Y \approx 0.46$. $M_{\rm env}$, and $M_{\rm H}$, are reduced (and the core mass correspondingly increased) by continuing hydrogen burning. Mass loss does scarcely reduce the total mass (see Sect. 2.1).

At $T_{\rm eff} = 5000$ K and 10000 K, resp., after the end of the RGB evolution the envelope masses of the Pop. I He-WD models are quite large, varying between $2 \cdot 10^{-3}{\rm M}_\odot$ and $50 \cdot 10^{-3}{\rm M}_\odot$ (see Table 1). It's noteworthy that $M_{\rm env}$ would be even larger for lower metallicity (Castellani et al. 1994).

Fig. 1 shows the complete evolutionary tracks of all sequences down to about $T_{\rm eff} \approx 4000$ K and $L \approx 10^{-4}\ {\rm L}_\odot$. The corresponding data[1] are given in Table 5-11. Only for two model sequences, 0.234 ${\rm M}_\odot$ and 0.259 ${\rm M}_\odot$, we found thermal instabilities of the hydrogen-burning shell when CNO burning ceases (e.g. Kippenhahn et al. 1968; Iben & Tutukov 1986). The hook-like inversions on the cooling tracks for $M = 0.300$ and $M = 0.331\ {\rm M}_\odot$ are also due to the onset of unstable burning. Full-scale instabilities are, however, avoided because the shell regions cool off too effectively. A detailed discussion of the properties of these hydrogen flashes is deferred to a separate paper. Here we only note that we adjusted our numerical time steps properly in order to resolve these flash phases with satisfactory accuracy. It is interesting to remark that no instabilities occurred below $M \lesssim 0.20\,{\rm M}_\odot$. The existence of a lower limit for the occurrence of hydrogen flashes, which has been predicted by Webbink (1975), has important ramifications for any discussions of the evolution of low-mass white dwarf companions of millisecond pulsars, as will be shown below.

Before discussing the properties of our helium white dwarf models, the influence of different input physics should briefly be reported. Concerning treatment of nuclear reactions we found no significant differences between tracks (or mass-radius relations) using the nuclear network and those only calculated with equilibrium rates for the four most important elements (H, He, C, O).

The comparison between tracks calculated with OPAL and the older CS opacities yielded, in short, the following differences:

- A well known shift of the RGB locus towards higher effective temperatures for CS opacities.
- Slightly larger turn-around temperatures for the CS post-RGB tracks. For example, a CS model sequence with $M = 0.412\ {\rm M}_\odot$ reached $\log T_{\rm eff} = 4.915$, the corresponding OPAL model ($M = 0.414\,{\rm M}_\odot$) only $\log T_{\rm eff} = 4.911$.
- The opacity effects on the locations of the cooling tracks as well as on the mass-radius relation and envelope masses were found to be small. Accordingly, the opacities seem not to be a critical parameter for the determination of the mass-radius relation (for given metallicity).
- White dwarf cooling ages are, as expected, significantly effected by the opacities. Models calculated with CS opacities have shorter cooling ages than those calculated with OPAL. The influence, however, is only noticeable in our more massive models where hydrogen burning is less dominant (see next section).

3.1. White dwarf cooling properties

For CO white dwarfs it is well known that the energy contribution of nuclear burning drops rapidly below the gravothermal energy release (compressional heating plus cooling) when the cooling branch is reached (Iben & Tutukov 1984b; Koester & Schönberner 1986; Blöcker 1995b). In contrast, full evolutionary calculations for helium white dwarfs show that hydrogen shell burning still plays a significant role on the cooling branch leading to hydrogen shell flashes for certain masses (e.g. Kippenhahn et al. 1968, Iben & Tutukov 1986, Castellani & Castellani 1993). The present calculations illustrate that hydrogen shell burning remains the main energy source down to temper-

[1] Tables 5-11 are only available in electronic form at the CDS via ftp 130.79.128.5.

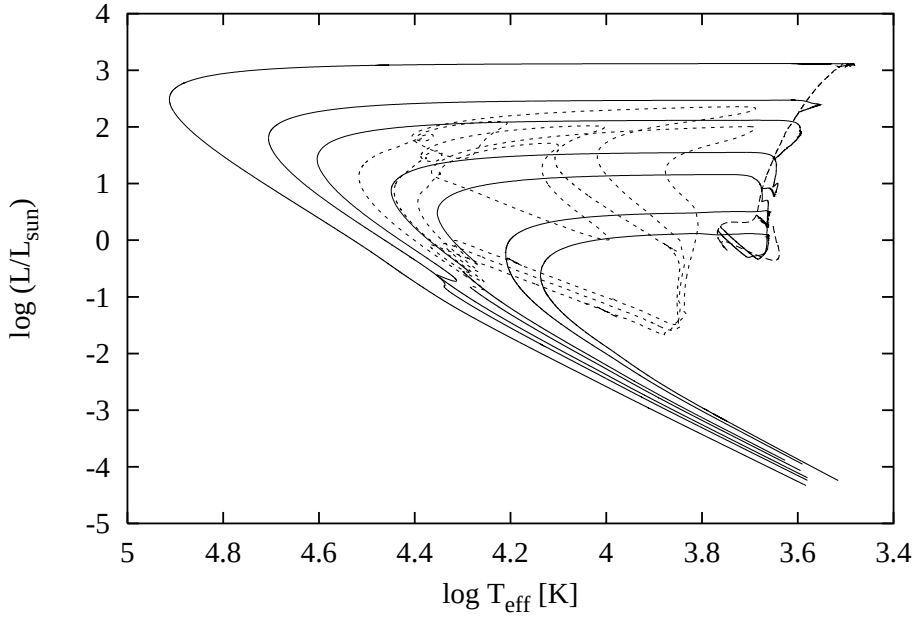

Fig. 1. HRD with complete evolutionary tracks of RGB remnants with different masses (from top: 0.414, 0.331, 0.300, 0.259, 0.234, 0.195, 0.179 $\mathrm{M}_\odot$). The long-dashed curve shows the evolutionary track of the 1 $\mathrm{M}_\odot$ star we used for abstracting the remnants by mass loss (see Sect. 2.1). The short-dashed loops mark the redward short excursions due to hydrogen shell flashes that occurred for the 0.259 and 0.234 $\mathrm{M}_\odot$ sequences when the CNO cycle is shut off.

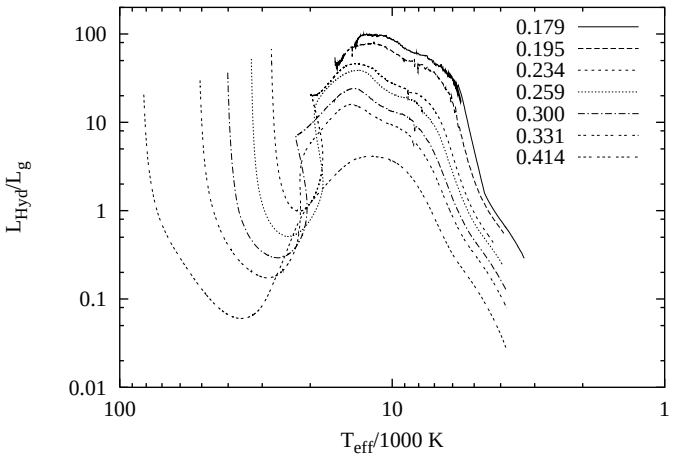

Fig. 2. Ratio of hydrogen to gravothermal luminosity as a function of $T_{\rm eff}$ for He-WDs of different masses.

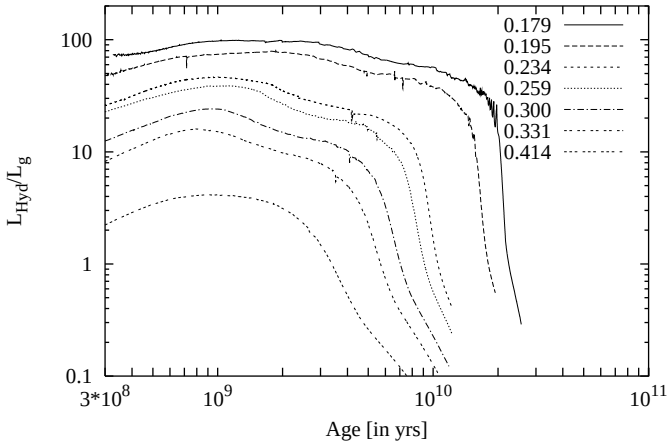

Fig. 3. Ratio of hydrogen to gravothermal luminosity as a function of the cooling age τ. Only the lower parts of the respective cooling curves ($T_{\rm eff} < 15000 \ldots 18000$ K) are plotted. The ages are counted from $T_{\rm eff} = 10\,000$ K ($M < 0.2\,\mathrm{M}_\odot$) and $T_{\rm eff} = 5\,000$ K ($M > 0.2\,\mathrm{M}_\odot$) on the (horizontal) post-RGB branch shown in Fig. 1.

atures well below $T_{\rm eff} = 10\,000$ K on the cooling branch. For demonstration, the temperatures in the burning shells are listed in Table 2. Also given are the corresponding envelope masses. The comparison with those at maximum effective temperatures illustrates clearly the significance of hydrogen burning.

Fig. 2 shows the ratio of the hydrogen shell luminosity, $L_{\rm Hyd}$, to the gravothermal luminosity, $L_{\rm g}$, for our helium-white dwarf sequences as a function of $T_{\rm eff}$. The shell flashes are omitted for clarity. Fig. 3 shows the same ratio as a function of the cooling age τ.

The left part of Fig. 2 indicates a rapid drop of $L_{\rm Hyd}/L_{\rm g}$ due to the decline of CNO burning right after the models have entered their cooling branches. At lower luminosities and temperatures, $L_{\rm Hyd}/L_{\rm g}$ exceeds unity again, entirely due to pp burning (see below). This phase of dominant hydrogen burning lasts for about 20 Gyr for the two least massive models (see Fig. 3). Even the 0.414 $\mathrm{M}_\odot$ model burns hydrogen for about 3 Gyr until gravothermal energy release finally resumes.

A more detailed picture of the temporal evolution of the different luminosity contributions (Figs. 4 and 5) reveals that at higher luminosities almost the entire energy production comes from shell CNO burning. At about $\tau \approx 2{\cdot}10^8$ yr ($0.195\,\mathrm{M}_\odot$) and $\tau \approx 1 \cdot 10^5$ yr ($0.414\,\mathrm{M}_\odot$) the cooling branch is reached, and L, $L_{\rm Hyd}$ and $L_{\rm CNO}$ start to decrease, slowly in the low-mass model, but very rapidly in the $0.414\,\mathrm{M}_\odot$ model. In the less massive models hydrogen burning via the pp chains remains the predominant luminosity contribution for more than 10 Gyr until finally gravothermal energy release starts to take over (see Fig. 4). Since unstable burning is restricted to a certain mass range the feature of continuing pp burning of low mass He-

Table 2. Temperatures at the center and the lower and upper boundary of the hydrogen burning shell for our different white dwarf models at $T_{\rm eff} = 10\,000$ K on the cooling branch. $T_{\rm bot}$ and $T_{\rm top}$ are the temperatures (in K) of those layers where the energy generation rate for hydrogen burning, $\epsilon_{\rm H}$, has dropped to 1 % of the maximum value. $\rm M_{env,knee}$ and $\rm M_{env}$ are the envelope masses at maximum effective temperature ($T_{\rm eff,knee}$) and at $T_{\rm eff} = 10\,000$ K on the cooling branch, resp. $L_{\rm knee}$ is the surface luminosity corresponding to $T_{\rm eff} = T_{\rm eff,knee}$.

$M/\rm M_\odot$	$\log(T_{\rm c}/\rm K)$	$\log(T_{\rm bot}/\rm K)$	$\log(T_{\rm top}/\rm K)$	$\frac{\rm M_{env}}{10^{-3}\rm M_\odot}$	$\frac{\rm M_{env,knee}}{10^{-3}\rm M_\odot}$	$\log T_{\rm eff,knee}/\rm K$	$\log(L_{\rm knee}/L_\odot)$
0.179	7.092	7.086	6.796	1.460	5.369	4.1372	-0.6202
0.195	7.070	7.068	6.784	1.184	5.214	4.2100	-0.2262
0.234	7.039	7.029	6.766	0.744	2.836	4.4430	0.8708
0.259	7.022	7.011	6.748	0.666	2.593	4.5168	1.1283
0.300	7.000	6.988	6.730	0.529	1.652	4.6038	1.4364
0.331	6.987	6.972	6.721	0.438	1.216	4.7053	1.7950
0.414	6.959	6.934	6.704	0.317	0.612	4.9124	2.4873

WDs ($M \lesssim 0.2\rm M_\odot$) is particularly independent of the details in modelling the phase of hydrogen shell flashes (e.g. the mass loss during the reexpansion phase due to Roche lobe overflow). For more massive models, pp burning stays important only for a few Gyr (Fig. 5).

The more gradual transition from CNO burning to pp burning is typical for less massive He-WDs. The more massive models show a rapid, more step-like shaped transition, very similar to the situation found in CO-WDs (Blöcker 1995b). Figs. 4 and 5, together with Fig. 2, also demonstrate that neither the gravothermal contribution nor the energy loss via neutrinos plays a significant role in the cooling history of He-WDs with $M \lesssim 0.2\,\rm M_\odot$ for ages $\tau \lesssim 10$ Gyr.

Fig. 6 illustrates how the the ratio $L_{\rm CNO}/L_{\rm pp}$ varies during the course of evolution. The hooks indicate the onset of unstable CNO burning, the flash loops are omitted for clarity. Fig. 6 elucidates also that pp burning becomes the dominant energy contribution for He-WDs below $T_{\rm eff} \approx 35\,000$ K for $M = 0.414\,\rm M_\odot$ and below $T_{\rm eff} \approx 18\,000$ K for $M = 0.234\,\rm M_\odot$. This coincides with the change from CNO to pp burning as can be seen from the minima in Fig. 2.

Summarizing, nuclear burning remains an important, if not dominant, energy source for helium-white dwarfs, even for temperatures of $T_{\rm eff} = 10\,000$ K and below. This is in particular true for objects with $M < 0.2\,\rm M_\odot$, like the companion of PSR J1012+5307. For example, Fig. 2 shows that for the WD companion of PSR J1012+5307 with $M \approx 0.2\,\rm M_\odot$ the ratio $L_{\rm Hyd}/L_{\rm g}$ is at least 50. The assumption $L_{\rm nuclear} \approx 0$ usually made in contraction models thus appears not to be appropriate for He-WDs. (e.g. Chin & Stothers 1971; Althaus & Benvenuto 1997).

However, Hansen & Phinney (1998a) and Benvenuto & Althaus (1998) did consider nuclear burning but found it of little importance. They did not model the evolution of the He-WD progenitor and had to make assumptions about the hydrogen envelope mass. Hansen & Phinney (1998a) selected an envelope mass of $M_{\rm H} = 3{\cdot}10^{-4}\,\rm M_\odot$ taken at some stage during the end of the second hydrogen shell flash from a $0.3\,\rm M_\odot$ model sequence calculated by Iben & Tutukov (1986). At this phase the envelope mass has already been considerably reduced by the hydrogen burning. Additionally, the Iben & Tutukov (1986) model had

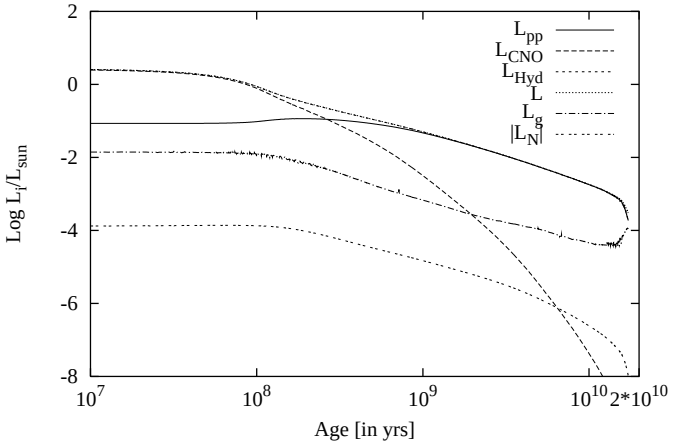

Fig. 4. Different luminosity contributions L_i as a function of cooling time τ for the 0.195 $\rm M_\odot$-sequence. Ages are counted from $T_{\rm eff} = 10\,000$ K on the horizontal post-RGB branch.

suffered from severe mass loss due to Roche lobe overflow during the expansion back to the RGB domain. Note that in models with $M \approx 0.3\rm M_\odot$ and such a small hydrogen envelope mass nuclear burning indeed becomes less important. However, as mentioned above, shell flashes do *not* occur for $M \lesssim 0.20\,\rm M_\odot$ which is the relevant mass range for the PSR J1012+5307 companion. The evolutionary models show that this object should have a hydrogen envelope of $M_{\rm H} \approx 10^{-3}\,\rm M_\odot$. Thus, the finding by Hansen & Phinney (1998a) that nuclear burning is negligible results from their choice of the hydrogen envelope mass which is not appropiate according to our models.

Additionally, the evolutionary history plays an important role as well since it determines the thermomechanical structure on the prevailing part of the cooling branch which is different if the pre-He-WD evolution is not considered. For instance, in contrast to full evolutionary calculations (e.g. Iben & Tutukov 1986, present paper) hydrogen burning can be found to be unimportant even for thick-envelope models ($M_{\rm H} \approx 10^{-3}\,\rm M_\odot$ for $M = 0.2\,\rm M_\odot$) if the pre-He-WD evolution is not considered (Benvenuto & Althaus 1998).

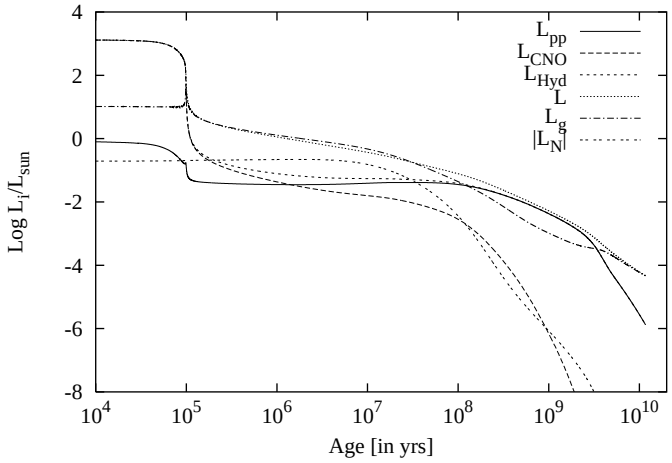

Fig. 5. Same as Fig. 5, but for the $0.414\,\mathrm{M}_\odot$-sequence. Ages are counted from $T_{\rm eff} = 5\,000$ K on the horizontal post-RGB branch.

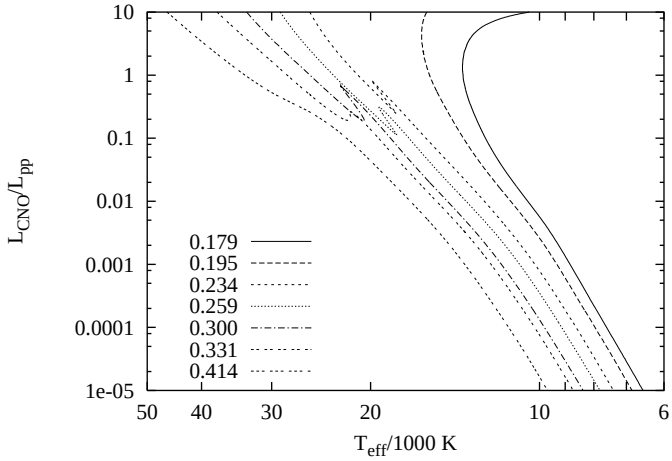

Fig. 6. Contribution of the two hydrogen burning reaction chains: ratio of luminosity due to the pp-chain ($L_{\rm pp}$) and due to the CNO-cycle ($L_{\rm CNO}$) as a function of $T_{\rm eff}$ on the WD cooling branch. The shell flashes are omitted for clarity.

3.2. Age and mass of the PSR J1012+5307 white dwarf companion

In order to estimate the influence of initial conditions on age and mass determinations for low-mass white dwarfs, we also calculated contraction models ($L_{\rm nuc} = 0$) with identical masses and chemical profiles as our evolutionary models. For that purpose we started with a homogeneous main sequence model of a given mass whose chemical profile was adapted over a series of about 50 models to the chemical structure of the corresponding evolutionary model at the beginning of the cooling branch (see Blöcker et al. 1997), but did not allow for hydrogen burning.

3.2.1. Cooling behaviour of helium-white dwarfs

Fig. 7 illustrates in a $\log g, T_{\rm eff}$ diagram the differences in the cooling properties between contraction models and one of our evolutionary models ($0.195\ \mathrm{M}_\odot$). At the position of the PSR J1012+5307 companion, our evolutionary model indicates an age of about 6 ± 1Gyr. In contrast, our contraction model as well as the models of Althaus & Benvenuto (1997) give only a cooling age of 0.4 Gyr, about a factor of 15 smaller and in serious conflict with the pulsar's spin-down age. Note that the contraction models agree in the cooling age but differ considerably in the mass-radius-relation (see Sect. 3.2.2), since Althaus & Benvenuto (1997) used $M_{\rm H} = 0$ while we took the same $M_{\rm H}$ as in the corresponding evolutionary model.

A more detailed view of the cooling behaviour of our evolutionary models is given in Fig. 8 which shows the tracks as well as the corresponding isochrones in the $\log g$ – $\log T_{\rm eff}$ plane. Note that hydrogen burning leads to different slopes of the isochrones for CO- and He-WDs. Usually, more massive white dwarfs cool faster then less massive ones. For He-WDs, however, the reverse is true. Due to the increasing importance of nuclear burning with decreasing mass, the less massive ones are considerably older than the more massive ones, at a given temperature below about 10 000 K. Hence, the isochrones of He-WDs run almost perpendicular to those of CO-WDs, and an extrapolation of cooling times of CO-WDs into the He-WD regime would give significantly lower cooling ages, close to those of the contraction models.

As already mentioned above, our evolutionary models predict a cooling age of 6 ± 1Gyr for the white dwarf companion of PSR J1012+5307, which is in good agreement with the estimated pulsar's spin-down age of 7 Gyr, and also with age estimates of Alberts et al. (1996) who also included nuclear burning.

Thus, evolutionary models for low-mass white dwarfs which start from explicit model calculations of the progenitors evolution seem to indicate that neither a modification of the theory of field decay as proposed by Burderi et al. (1996) nor the consideration of initial spin periods close to the present one are necessary to resolve the apparent age discrepancy between the two components of PSR J1012+5307.

3.2.2. Mass-radius relations of helium-white dwarfs

The mass-radius relation according to our models is shown in Fig. 9 and also listed in Table 3. For intermediate temperatures some distortions can be seen where hydrogen flashes with the associated high burning rates lead to a substantial reduction of the envelope mass. A more thorough discussion will be presented in a forthcoming paper. Important for the interpretation of observations is the remarkable temperature dependence of the radii even at the low temperature end.

The structural differences between evolutionary and purely contracting white dwarf models influence the evolutionary tracks as well. For selected masses the tracks of evolutionary and contracting white dwarfs with identical chemical structures are plotted in Fig. 10. The long-dashed line in the figure connects roughly the loci where the tracks of evolutionary and contraction models do converge. In the regime above this line the thermo-mechanical structure of white dwarfs does depend on their (assumed) evolutionary history. This has important consequences

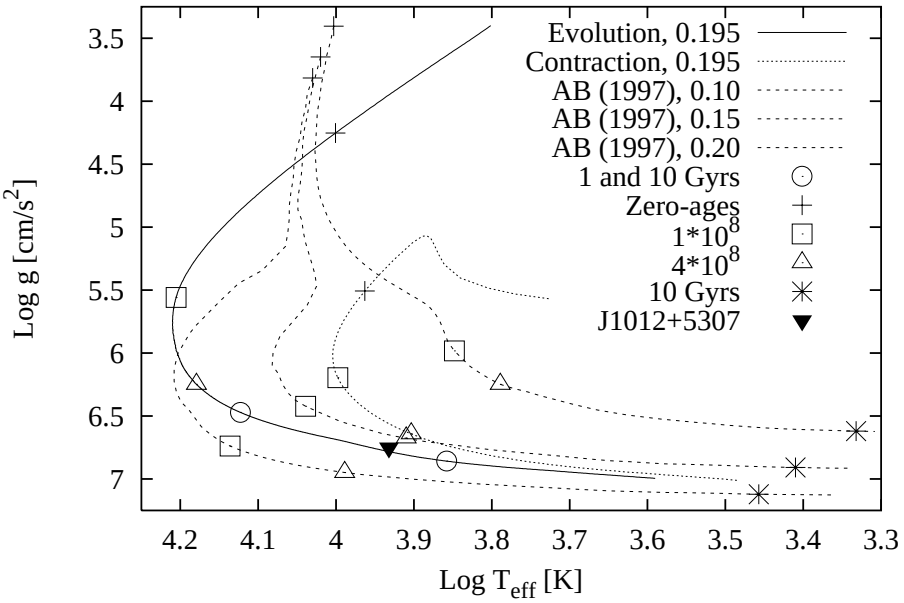

Fig. 7. $\log g - \log T_{\rm eff}$ diagram with our tracks for $M = 0.195\,{\rm M}_\odot$ with and without consideration of nuclear burning (continuous and dotted line, see text). Also shown are the tracks of Althaus & Benvenuto (1997) for $M = 0.1, 0.15$ and $0.2\,{\rm M}_\odot$ (AB, dashed lines) as well as time marks for different cooling stages as indicated. Additional circles mark cooling ages of our evolutionary model of 1 and 10 Gyr, resp. All ages are counted from a pre-white dwarf stage close to $T_{\rm eff} = 10\,000$ K. The filled triangle marks the position of the PSR J1012+5307 white dwarf.

Table 3. Radii for He-WDs for different masses and effective temperatures (see also Fig. 9). The radii are given in solar units.

	$M/{\rm M}_\odot$						
	0.179	0.195	0.234	0.259	0.300	0.331	0.414
$T_{\rm eff}/{\rm K}$							
40 000	-	-	-	-	0.0972	0.0525	0.0330
35 000	-	-	-	-	0.0626	0.0460	0.0301
30 000	-	-	-	0.0698	0.0512	0.0407	0.0267
25 000	-	-	0.0698	0.0523	0.0433	0.0353	0.0226
20 000	-	-	0.0505	0.0424	0.0284	0.0248	0.0196
15 000	-	0.0538	0.0322	0.0286	0.0244	0.0220	0.0182
10 000	0.0384	0.0332	0.0264	0.0244	0.0217	0.0201	0.0170
5 000	0.0261	0.0246	0.0219	0.0208	0.0192	0.0181	0.0159

for mass determinations from spectroscopy (see Blöcker et al. 1997). If an object's position lies above the line its mass will be overestimated by using simple contraction models with the same envelope masses as the corresponding evolurionary models. This fact is especially important for helium-white dwarfs with their low masses: The tracks of evolutionary and contraction models in the $\log g - \log T_{\rm eff}$-diagram merge only very late at rather low effective temperatures. For example, the merging of both $0.2\ {\rm M}_\odot$ tracks occurs at $\log T_{\rm eff} \approx 3.5$!

Although in the lower right part of Fig. 10 the thermomechanical structures of evolutionary and contracting models agree, the evolutionary speeds may be very different because hydrogen burning slows down the 'cooling' for the lower masses.

The possible differences in structure between evolutionary and contracting white dwarf models translate also into differences in the mass-radius relations, as demonstrated in Fig. 11. One can again see that according to contraction models the object's mass for given gravity is overestimated. However, the larger hydrogen envelope masses which result in our models from their evolutionary history have the effect to increase the masses derived from atmospheric parameters and mass-radius relation. Thus the two effects of contraction vs. evolutionary models (with regard to the treatment of $L_{\rm nuc} = 0$) and smaller, mass independent envelope masses vs. evolutionary (thicker, mass dependent) envelope masses compensate each other to a certain extent. This can be seen from Fig. 12 which gives mass-radius relations of different origin in order to compare the mass determination of the PSR J1012+5307 companion. The deviations from the $T = 0$ K relation of Hamada & Salpeter (1961) for a pure helium composition demonstrate the well known importance of finite temperature effects in the equation of state, especially for the low-mass WDs. For a surface gravity $\log g = 6.75$ of the pulsar's companion that relation yields $M \approx 0.12\ {\rm M}_\odot$ which is close to the lower limit $M \cdot \sin i = 0.11\,{\rm M}_\odot$. The differences between our mass-radius relation and those of van Kerkwijk et al. (1996) and Althaus & Benvenuto (1997) are mainly due to the larger envelope masses (i.e. thicker hydrogen layers) predicted from our evolutionary models. For example, van Kerkwijk et al. (1996) interpolated between the Hamada & Salpeter relation based on pure helium cores ($M_{\rm H} = 0$) and that based on

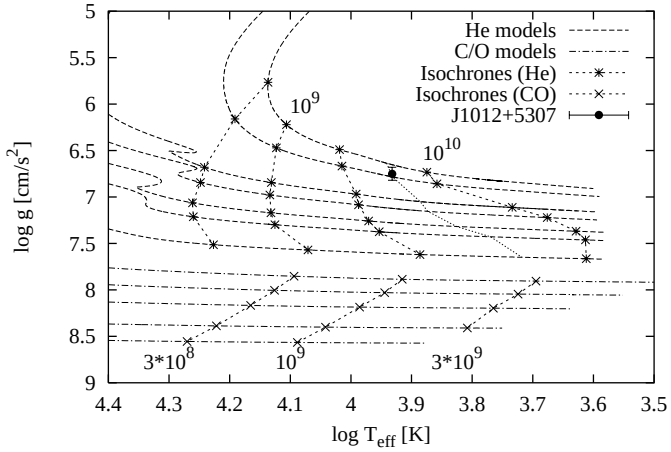

Fig. 8. $\log g - \log T_{\rm eff}$ diagram with our evolutionary tracks for He-WDs ($M = 0.179$, 0.195, 0.234, 0.259, 0.300, 0.331, $0.414 M_\odot$ and for CO-WDs ($M = 0.524$, 0.605, 0.696, 0.836, $0.940 M_\odot$; Blöcker 1995b). The masses increase from top to bottom. Also shown is the locus of the companion of the millisecond pulsar PSR J1012+5307 as given by van Kerkwijk et al. (1996). Isochrones are shown for $3 \cdot 10^8, 1 \cdot 10^9, 3 \cdot 10^9$, and 10^{10} yr (from left to right, last isochrone only for He-WDs). The isochrones for the He-WDs are turned over and shifted to the left because hydrogen burning slows down the evolution so much. The dotted isochrone of $6 \cdot 10^9$ yr fits the position of the PSR J1012+5307 companion.

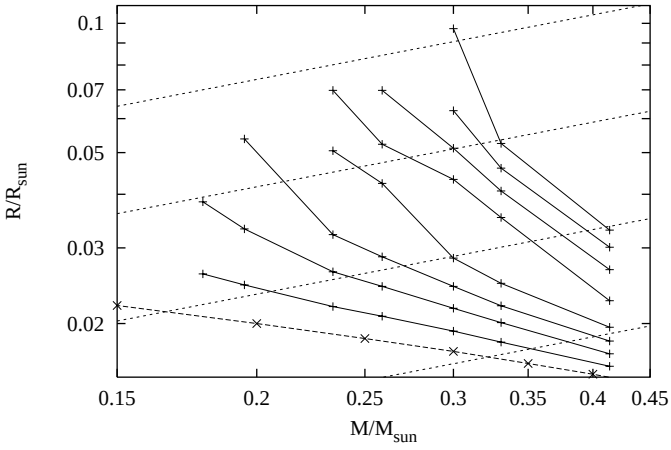

Fig. 9. Mass-radius relation for He-WDs at different effective temperatures, calculated from our evolutionary models from $T_{\rm eff} = 40000$ K (upper line) down to $T_{\rm eff} = 5000$ K (lower line) in steps of $\Delta T_{\rm eff} = 5000$ K (Table 3). For comparison also the $T = 0$ K relation of Hamada & Salpeter (1961) for pure helium models (dashed line) is given. Along the dotted lines gravity is constant, with (from above) $\log g = 6.0, 6.5, 7.0$ and 7.5). Temperatures larger than 10 000 K are not reached by RGB remnants of too low a mass (see Fig. 1). The irregularities around $T_{\rm eff} = 20000$ K are due to thermal instabilities in the hydrogen burning shell as explained in the text.

models from Wood (1994) with 'thick', but constant hydrogen layers ($M_{\rm H} = 10^{-4} M_*$). Our evolutionary calculations, however, revealed a large dependence of envelope thicknesses on total masses: $M_{\rm H}$ drops from $\approx 10^{-3}\,{\rm M}_\odot$ for $M = 0.2\,{\rm M}_\odot$ to $M_{\rm H} \approx 10^{-4}\,{\rm M}_\odot$ for a C/O WD with $M = 0.6\,{\rm M}_\odot$, the heaviest

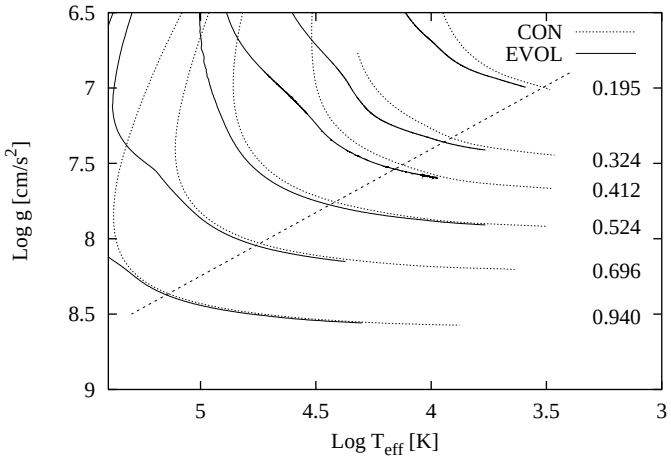

Fig. 10. $\log g - \log T_{\rm eff}$-diagram with WD tracks according to evolutionary models (i.e. with consideration of nuclear burning, solid curves) and contraction models (i.e. no nuclear burning, dotted curves) with the same masses and chemical structures for the masses as indicated by the labels. The evolutionary tracks are either from this study or from Blöcker (1995b) for the larger masses. The contraction models are from Blöcker et al. (1997). The dashed line divides the diagram roughly in two parts: in the lower right part contraction and evolutionary models have virtually the same thermo-mechanical structure.

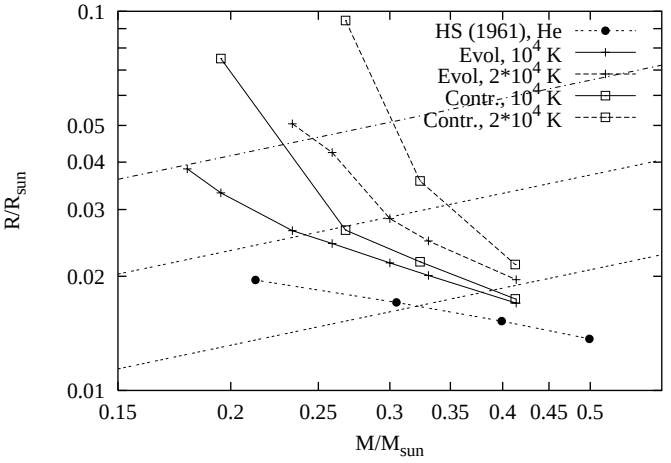

Fig. 11. Mass-radius relation derived from evolutionary (crosses) and contraction models (squares) with identical chemical profiles at $T_{\rm eff} = 10\,000$ K and 20 000 K. Also given are the $T = 0$ K relation of Hamada & Salpeter (1961) (dots) and lines of constant surface gravities (dashed, from above: $\log g = 6.5, 7.0, 7.5$).

He-WDs with $M \approx 0.45\,{\rm M}_\odot$ having about $M_{\rm H} = 10^{-3.75}\,{\rm M}_\odot$ (see Table 2, Blöcker et al. 1997). Note that in contrast to Figs. 10 and 11 the contraction models of Althaus & Benvenuto (1997) give smaller white dwarf masses compared to our evolutionary models due to the much smaller envelope masses (in this case $M_{\rm H} = 0$).

As can be seen from Fig. 12, our mass-radius relation yields a mass of $M = 0.19 \pm 0.02\,{\rm M}_\odot$ for the white dwarf companion of PSR J1012+5307, using $\log g = 6.75$. This is larger than the value quoted by van Kerkwijk et al. (1996) and Callanan et al. (1998) but within the mass range $M_{\rm He-WD} = 0.13 \ldots 0.21\,{\rm M}_\odot$

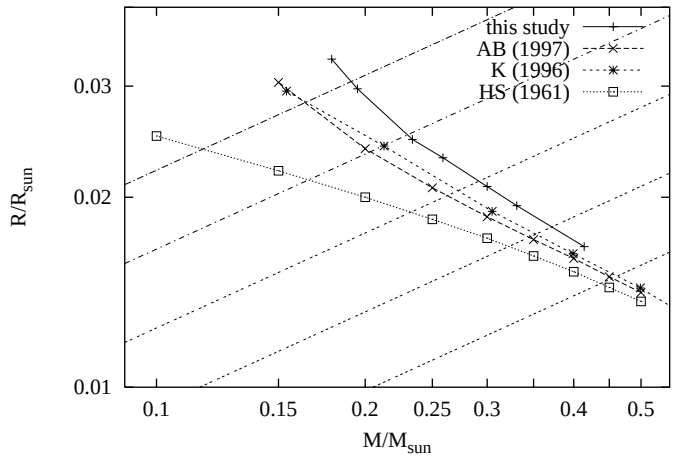

Fig. 12. Mass-radius relation at $T_{\rm eff} = 8550$ K, relevant for the mass determination of the PSR J1012+5307) companion, from different authors: AB = Althaus & Benvenuto (1997), K = van Kerkwijk et al. (1996); HS = Hamada & Salpeter (1961). Lines for constant surface gravity are also given, starting from $\log g = 6.75$ (upper line, relevant for PSR J1012+5307) to $\log g = 7.75$ in steps of $\Delta \log g = 0.25$.

Table 4. Spectroscopic results, i.e. $\log g$ and $T_{\rm eff}$, and derived masses, $M_{\rm He-WD}$, for the PSR J1012+5307 He-WD. The lower part gives the He-WD mass from the present work ($M_{\rm He-WD,PW}$) derived from the respective spectroscopic analysis. $M_{\rm pulsar,K}$ is the pulsar mass based on the mass ratio $M_{\rm pulsar}/M_{\rm He-WD} \approx 9.5 \pm 0.3$ (van Kerkwijk et al. 1998, priv. comm.) and $M_{\rm He-WD,PW}$. $M_{\rm pulsar,C}$ is the pulsar mass based on the mass ratio from Callanan et al. (1998) ($M_{\rm pulsar}/M_{\rm He-WD} \approx 10.5 \pm 0.5$) and $M_{\rm He-WD,PW}$.

	Callanan et al. (1998)	van Kerkwijk et al. (1996)
$\log g[{\rm cm/s^2}]$	6.34 ± 0.20	6.75 ± 0.07
$T_{\rm eff}$ [K]	8670 ± 300	8550 ± 25
$M_{\rm He-WD}[{\rm M}_\odot]$	0.16 ± 0.02	0.16 ± 0.02
$M_{\rm He-WD,PW}[{\rm M}_\odot]$	0.15 ± 0.02	0.19 ± 0.02
$M_{\rm pulsar,K}[{\rm M}_\odot]$	1.43 ± 0.25	1.81 ± 0.25
$M_{\rm pulsar,C}[{\rm M}_\odot]$	1.59 ± 0.30	2.00 ± 0.30

given by Hansen & Phinney (1998b). Similarly, $M = 0.16\,{\rm M}_\odot$ follows from the Althaus & Benvenuto (1997) relation. With the spectroscopic analysis from Callanan et al. (1998) a mass of $M = 0.15 \pm 0.02\,{\rm M}_\odot$ follows by extrapolating our mass-radius relation.

With the mass ratio $M_{\rm pulsar}/M_{\rm He-WD} \approx 9.5 \pm 0.3$ (van Kerkwijk 1998, priv. comm.) the pulsar's mass can be estimated: $M_{\rm He-WD} = 0.15\,{\rm M}_\odot$ gives $M_{\rm pulsar} \approx 1.43 \pm 0.25\,{\rm M}_\odot$, close to the canonical pulsar mass of $\approx 1.5\ {\rm M}_\odot$. On the other hand, $M_{\rm He-WD} = 0.19\ {\rm M}_\odot$ gives $M_{\rm pulsar} \approx 1.81 \pm 0.25\,{\rm M}_\odot$. Slightly increased values for $M_{\rm pulsar}$ are obtained if the mass ratio $M_{\rm pulsar}/M_{\rm He-WD} \approx 10.5 \pm 0.5$ from Callanan et al. (1998) is applied. A summary of the results for the mass determination of the components of the PSR J1012+5307 system is given in Table 4.

4. Summary and conclusions

We have computed a representative grid of evolutionary white dwarf models of low mass for solar composition whose structure is consistent with their earlier history of being remnants of the first giant branch. Though such models have already been presented in the literature for isolated cases, our calculations are the first that cover a whole range of masses. These models allowed then to draw several important conclusions:

- We found thermal instabilities due to hydrogen burning via the CNO cycle in a geometrically thin shell (hydrogen shell flashes) at the beginning of the cooling branch of our evolutionary tracks. It turned out, however, that these shell flashes do occur only within a limited mass range, $M = 0.21 \ldots 0.30\ {\rm M}_\odot$, independently from the detailed input physics used.
- The cooling speed is reduced by ongoing hydrogen burning at the bottom of the envelope via the pp chains. This effect is the more pronounced the less massive the models are and may slow down the cooling down to 10 000 K by up to a factor of about 40. This is important for age determinations of binary systems containing helium-white dwarfs by using the cooling age of the white dwarf components. The employment of inconsistent white dwarf models may give grossly wrong results in the sense that ages are underestimated.
  We re-determined the age of the white dwarf component in the PSR J1012+5307 system with our evolutionary models and found an age of 6 ± 1Gyr, 15 times larger than that estimated from contraction models, but in excellent agreement with the pulsar's spin-down age of about 7 Gyr. We confirm the results of Alberts et al. (1996) who also found 7 Gyr based on their white dwarf models.
- Our evolutionary models predict an inverse correlation of envelope mass with total mass, which is a continuation of the correlation already apparent for the more massive white dwarfs with carbon-oxygen cores (Blöcker et al. 1997). At the low mass end, the evolutionary envelope masses are at least ten times larger than the often ad hoc assumed values for contraction models. Translated into a mass-radius relation, these larger envelope masses lead to correspondingly higher mass estimates for any given $g, T_{\rm eff}$, and especially for the white dwarf companion of PSR J1012+5307 a mass of $M = 0.19\ {\rm M}_\odot$ follows, instead of $M = 0.16\,{\rm M}_\odot$ by using existing contraction models.

Acknowledgements. T.B. and F.H. acknowledge funding by the Deutsche Forschungsgemeinschaft (grants Ko 738/12 and Scho 394/13). We thank Detlev Koester for many helpful discussions on white dwarfs and Marten van Kerkwijk for constructive remarks on the manuscript.

References

Alberts F., Savonije G.J., van der Heuvel E.P.J., 1996, Nat. 380, 676
Alexander D.R., Ferguson J.W., 1994, ApJ 437, 879
Althaus L.G., Benvenuto O.G., 1997, ApJ 477, 313

Bailes, M., Lorimer, D., 1995, in: Millisecond pulsars: a decade of surprises, A. S., Fruchter, M. Tavani, D. C. Backer (eds.), ASP Conf. Ser. 72
Benvenuto, O. G., Althaus, L. G., 1998, MNRAS 293, 177
Blöcker T. 1995a, A&A 297, 727
Blöcker T. 1995b, A&A 299, 755
Blöcker T., Herwig F., Driebe T., Bramkamp H., Schönberner D., 1997, in: White Dwarfs, Isern J., Hernanz M., Garcia-Berro E. (eds.), Kluwer, Dordrecht, p. 57
Bragaglia A., Greggio L., Renzini A., D'Odorico S., 1990, ApJ 365, L13
Burderi L., King A.R., Wynn G.A., 1996, MNRAS 283, L63
Callanan, P. J., Garnavich, P. M., Koester, D., 1998, MNRAS 298, 207
Cameron A. G. W., Iben I. Jr., 1986, ApJ 305, 228
Camilo F., 1996, in: *Pulsar Timing, General Relativity and the Internal Structure of Neutron Stars*, Proc. Coll. held at the Roy. Netherlands Academy of Arts & Science, Eds.: Z. Arzoumanian, E. P. J. van den Heuvel & J. van Paradijs (Amsterdam: North Holland), in press.
Camilo F., Thorsett S. E., Kulkarni S. R., 1994, ApJ 421, L15
Camilo F., Nice D. J., Shrauner J. A., Taylor J. H., 1996, ApJ 469, 819
Castellani M., Castellani V., 1993, ApJ 407, 649
Castellani V., Luridiana V., Romaniello M., 1994, ApJ 428, 633
Chin C.-W., Stothers R., 1971, ApJ 163, 555
Cox A.N., Stewart J.N., 1965a, ApJS 11, 1
Cox A.N., Stewart J.N., 1965b, ApJS 11, 22
Cox A.N., Stewart J.N., 1970, ApJS 19, 243
El Eid, M., 1994, A&A 285, 915
Ergma E., Sarna M.J., 1996, MNRAS 280, 1000
Gianonne P., Refsdal S., Weigert A., 1970, A&A 4, 428
Hamada T., Salpeter E.E., 1961, ApJ 134, 683
Hansen B.M.S., Phinney E.S., 1998a, MNRAS, 294, 557
Hansen B.M.S., Phinney E.S., 1998b, MNRAS, 294, 569
Iben I. Jr., Renzini A., 1983, ARAA 21, 271
Iben I. Jr., Tutukov A.V., 1984a, ApJS 54, 335
Iben I. Jr., Tutukov A.V., 1984b, ApJ 282, 615
Iben I. Jr., Tutukov A.V., 1986, ApJ 311, 742
Iben I. Jr., Tutukov A.V., Yungelson L.R., 1995, ApJS 100, 233
Iglesias C.A., Rogers F.J., 1996, ApJ 464, 943
Iglesias C.A., Rogers F.J., Wilson B., 1992, ApJ 397, 717
van Kerkwijk M.H., Bergeron P., Kulkarni S.R., 1996, ApJ 467, L89
Kippenhahn R., Weigert A., 1967, Z. f. Astr. 65, 251
Kippenhahn R., Kohl K., Weigert, A., 1967, Z. f. Astr. 66, 58
Kippenhahn R., Thomas H.-C., Weigert A., 1968, Z. f. Astr. 69, 256
Koester D., Schönberner D., 1986, A&A 154, 125
Lorimer D.R., Festin L., Lyne A.G., Nicastro L., 1995, Nat 376, 393
Lyne, A.G. 1995, in: Compact stars in binaries, IAU Symp. 165, E. P. J. van der Heuvel (ed.)
Lyne, A.G. 1996, in: Proc. of the 7th M. Grossmann Meeting, in press
Maeder, A., Meynet, G., 1989, A&A 210, 155
Marsh T.R., 1995, MNRAS 275, L1
Marsh T.R., Dillon V.S., Duck S.R., 1995, MNRAS 275, 828
Moran C., Marsh T.R., Bragaglia A., 1997, MNRAS 288, 538
Nicastro L., Lyne A.G., Lorimer D.R. et al., 1995, MNRAS, 273, L68
Phinney E.S., Kulkarni S.R., 1994, ARA&A 32, 591
Rappaport S., Podsiadlowski P., Joss P.C., Di Stefano R., Han Z., 1995, MNRAS 273, 731
Ray P. S., Thorsett S. E., Jenet F. A., et al. 1996, ApJ 470, 1103
Refsdal S., Weigert A., 1969, A&A 1, 167
Reimers D., 1975, Mem. Soc. Sci. Liege 8, 369
Saffer R.A., Liebert J., Olszewski E., 1988, ApJ 334, 947
Saffer R.A., Livio, M., Yungelson, L. R., 1998, ApJ, accepted
Sarna M.J., Marks P.B., Connon Smith R., 1996, MNRAS 279, 88
Schönberner D., 1979, A&A 79, 108
Schönberner D., 1983, ApJ 271, 708
Shore, S. N., Livio, M., van der Heuvel, E. P. J., 1994: in *Interacting Binaries*, Saas-Fee Course 22, Swiss Soc. Astrophys. Astron., H. Nussbaumer & A. Orr (eds.), Springer (Berlin)
Slattery W.L., Doolen G.D., DeWitt H.E., 1982, Phys. Rev. A26, 2255
Tauris T.M., 1996, A&A 315, 453
Tauris T.M., Bailes M., 1996, A&A 315, 432
Vassiliadis E., Wood P.R., 1993, ApJ 413, 641
Vassiliadis E., Wood P.R., 1994, ApJS 92, 125
Verbunt F., 1993, ARA&A 31, 93
Webbink R.F., 1975, MNRAS 171, 555
Webbink R.F., 1984, ApJ 277, 355
Webbink R.F., Rappaport S., Savonije G.J., 1983, ApJ 270, 678
Wood M.A., 1994, in *White Dwarfs*, D. Koester & K. Werner (eds.), Springer, Berlin, p. 41